https://doi.org/10.15302/frontphys.2025.054201

RESEARCH ARTICLE

Higher-order anti-PT symmetry for efficient wireless power transfer in multiple-transmitter system

Likai Wang[1,#], Yuqian Wang[1,#], Shengyu Hu[1], Yong Sun[1], Haitao Jiang[1], Yunhui Li[2], Yaping Yang[1], Hong Chen[1], Zhiwei Guo[1,†]

[1]School of Physics Science and Engineering, Tongji University, Shanghai 200092, China

[2]Department of Electrical Engineering, Tongji University, Shanghai 201804, China

[#]These authors contributed equally to this work.

Corresponding author. E-mail: [†]2014guozhiwei@tongji.edu.cn

Received January 25, 2025; accepted March 26, 2025

Supporting Information

Supplementary Note A: Simulation of virtual coupling variation in a second-order anti-PT-symmetric system

The evolution of the κ_0 (virtual coupling) dimension in the second-order anti-PT-symmetric system can be further validated through simulations. By establishing an appropriate simulation model, we can gain a deeper understanding of the role of virtual coupling in the system and evaluate its impact on overall transfer efficiency, frequency stability, and bandwidth. Simulations can provide a more precise observation of the behavior of virtual coupling, which can be compared with experimental results to verify the theoretical predictions of the system. Here, we use the Advanced Design System (ADS) simulation software for validation. The parameters are kept the same as those in Fig. 1(c) of the main text, and the circuit is shown in Fig. 2(c) of the main text.

Here, $L_1 = L_3 = 230\,\mu H$, $C_1 = 8.32\,nF$, $C_2 = 15.24\,nF$, $\Delta = 15$ kHz.The virtual coupling strength is varied by sweeping the internal resistance value R=10Ω, 20Ω, 30Ω, 40Ω, 50Ω of port 1, and the results are shown in Fig. S1. It can be seen that as the virtual coupling increases, the reflection coefficient transitions from splitting to gradually merging. Figure S2 shows a comparison between the calculated and simulated results, and it can be observed that they match very well.

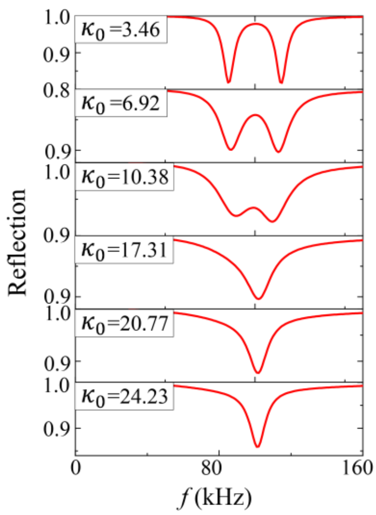

Fig. S1 The variation trend of the reflection coefficient corresponding to different virtual coupling.

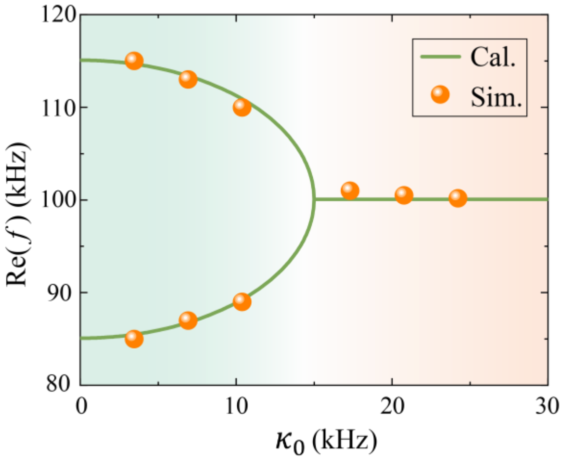

Fig. S2 The relationship between eigenfrequency and virtual coupling, with the spheres representing simulation results and the curve representing calculated results.

Supplementary Note B: Verification of the influence of neighboring coupling between transmitting coils

In the coupled transmitter (*Tx*) configuration illustrated in Fig. 2(b) of the main text, proximity-induced nearest-neighbor coupling between *Tx* coils constitutes an inherent design challenge. If not properly managed, this coupling can reduce the efficiency of the energy dissipation system and compromise the accuracy of the physical model. To address this, we implement a counter-winding configuration that generates mutual flux cancellation - a technique confirmed to suppress inter-coil coupling by 62.5% (from S_{21}= 0.24 to 0.09) through vector network analyzer (VNA) measurements in dual-port configuration using port1 and port2. Figure S3 systematically compares coupling characteristics under two operational states: (i) a = 0 cm: exhibits transmittance S_{21} = 0.24 at target frequency, corresponding to 5.76% energy flow (ii) a = 2 cm: demonstrates suppressed S_{21}=0.09, reducing energy transfer to 0.81% (0.09^2). These results indicate that, at a 2 cm separation, the energy dissipation flow and mutual influence between the coils are negligible. For the configuration in Fig. 2(a), the distance between the coils is much greater than 2 cm, so we do not discuss this case further.

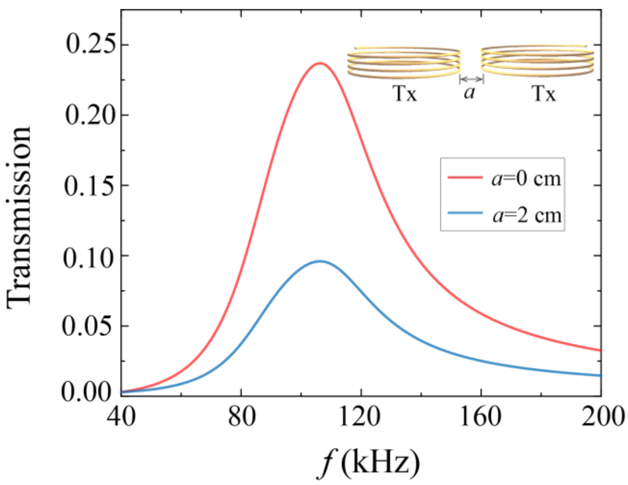

Fig. S3 Comparison of transmittance of neighboring coupling between two transmitting coils at different a.

Supplementary Note C: Conventional MTSR vs anti-PT-symmetric systems: comparative analysis of performance

The advantage of traditional multiple transmitter, single receiver (MTSR) lies in its tolerance to lateral misalignment and error-resistant performance. However, when comparing the efficiency with respect to two transmitters, it does not offer a significant advantage over a single transmitter system. In this work, we ingeniously combine anti-PT symmetry with the MTSR configuration, greatly enhancing its efficiency and robustness while retaining its original advantages. This approach significantly increases the potential and competitiveness of multi-transmitter, multi-receiver architectures for future applications.

Here we compare traditional MTSR with it:

$$\begin{aligned}\frac{da_1}{dt}&=\left[-i(\omega_0+\Delta)-g_1-\Gamma_1\right]a_1-i\kappa_1 a_3+\sqrt{2g_1}S_{a+}\\ \frac{da_3}{dt}&=(-i\omega_0-\gamma_1-\Gamma_3)a_3-i\kappa_1 a_1-i\kappa_2 a_2\\ \frac{da_2}{dt}&=\left[-i(\omega_0-\Delta)-g_2-\Gamma_2\right]a_2-i\kappa_2 a_3+\sqrt{2g_2}S_{b+}\end{aligned} \tag{S1}$$

To simplify the model, let $\kappa_1 = \kappa_2 = \kappa$, $g_1 = g_2 = g$. Neglecting the intrinsic loss $\Gamma_1 = \Gamma_2 = \Gamma_3 = 0$ and under the condition of zero reflection $S_{a-} = -S_{a+} + \sqrt{2g_1}a_1 = 0$, $S_{b-} = -S_{b+} + \sqrt{2g_2}a_2 = 0$, it can be obtained that the Hamiltonian is

$$H=\begin{pmatrix}\omega_0+ig & \kappa & 0\\ \kappa & \omega_0-i\gamma & \kappa\\ 0 & \kappa & \omega_0+ig\end{pmatrix} \tag{S2}$$

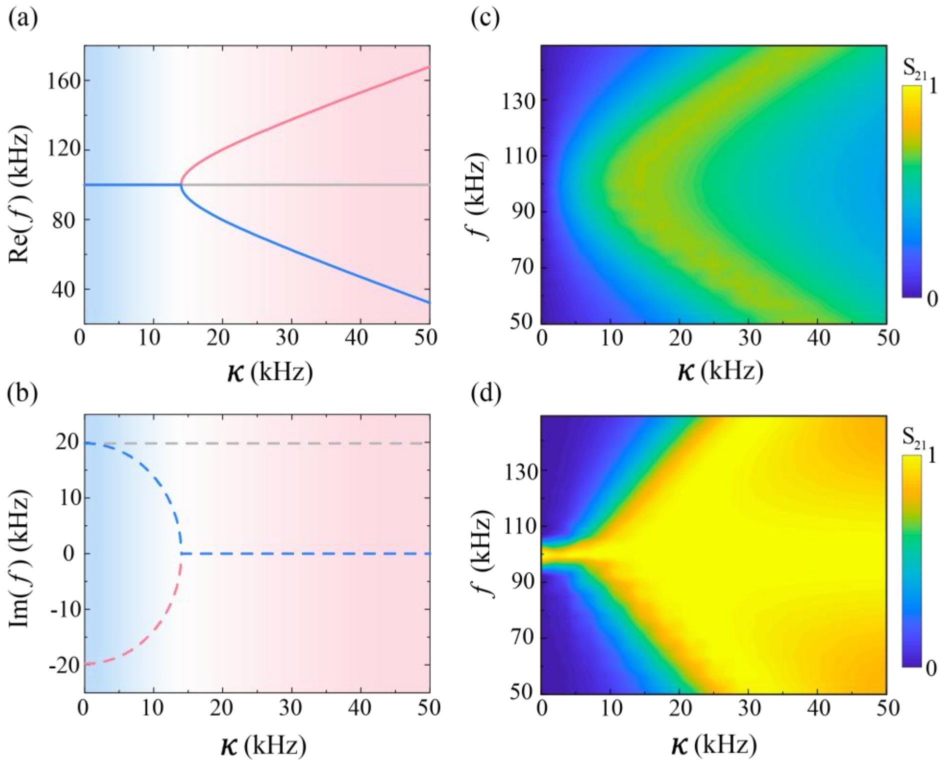

Fig. S4 Performance comparison between traditional MTSR system and anti-PT symmetric system. Traditional MTSR eigenvalues **(a)** Real part **(b)** Imaginary part. **(c)** Efficiency of traditional MTSR system. **(d)** Efficiency of anti-PT-symmetric system.

The real and imaginary parts of the eigenvalues of the traditional MTSR system are shown in Figs. S4(a) and (b), while the real and imaginary parts of the eigenvalues of the anti-PT-symmetric system are presented in Fig. 1(d) in the main text. In Figs. S4(a), (b) and (c), $g=\gamma$ and all other parameters are the same as the anti-PT-symmetric system mentioned in the main text. By comparison, it can be observed that the anti-PT-symmetric system always has eigenvalues with a zero imaginary part that are independent of frequency.

Its efficiency is (to simplify the calculation, let the strengths of two independent input sources be the same, $S_{a+}=S_{b+}=S_{1+}$):

$$\begin{aligned}\eta &= [\frac{S_{2-}}{2S_{1+}}]^2 \\ &= \frac{g}{2} Abs\left[\frac{2i\sqrt{2}g^{3/2}\kappa+2\sqrt{2}\sqrt{g}\kappa\omega-2\sqrt{2g}\kappa\omega_0}{g^3+2g\kappa^2-(3ig^2+2i\kappa^2)\omega-3g\omega^2+i\omega^3+(3ig^2+2i\kappa^2+6g\omega-3i\omega^2)\omega_0-3g\omega_0{}^2+3i\omega\omega_0{}^2-i\omega_0{}^3}\right]^2\end{aligned} \tag{S3}$$

Figures S4(c) and (d) show a comparison of the efficiency between the traditional MTSR system and the anti-PT-symmetric system. It is clearly observed that the efficiency of the anti-PT-symmetric system is significantly higher and exhibits a broader bandwidth.

Supplementary Note D: Higher-order anti-PT-symmetric WPT system

The proposed third-order anti-PT-symmetric WPT system has excellent scalability and can effectively meet the demand for simultaneous power supply to multiple devices in the Internet of things era. Through the MTSR configuration, the system can provide stable energy transfer to multiple devices at the same time. The third-order anti-PT-symmetry further enhances the system's frequency stability and broadband characteristics, enabling reliable operation under varying environmental conditions, particularly in the ever-changing IoT environment. As an example, consider extending it to a fifth-order system (which can theoretically be extended to higher orders), with the system adopting a two-transmitter, three-receiver configuration. The schematic diagram of its model is shown in Fig. S5. Its dynamic equations can be written as

$$\begin{aligned}\frac{da_1}{dt} &= \left[-i(\omega_0+\Delta)-g_1-\Gamma_1\right]a_1-i\kappa_1a_3-i\kappa_2a_4-i\kappa_3a_5+\sqrt{2g_1}S_+-\sqrt{g_1g_2}a_2 \\ \frac{da_3}{dt} &= (-i\omega_0-\gamma_1-\Gamma_3)\,a_3-i\kappa_1a_1+i\kappa_1a_3 \\ \frac{da_4}{dt} &= (-i\omega_0-\gamma_2-\Gamma_4)\,a_4-i\kappa_2a_1+i\kappa_2a_3 \\ \frac{da_5}{dt} &= (-i\omega_0-\gamma_3-\Gamma_5)\,a_5-i\kappa_3a_1+i\kappa_3a_3 \\ \frac{da_2}{dt} &= \left[-i(\omega_0-\Delta)-g_2-\Gamma_2\right]a_2+i\kappa_1a_3+i\kappa_2a_4+i\kappa_3a_5+\sqrt{2g_2}S_+-\sqrt{g_1g_2}a_1\end{aligned} \tag{S4}$$

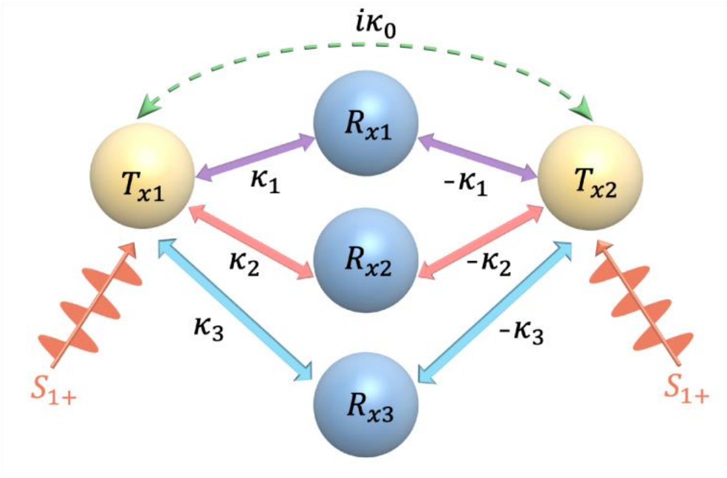

Fig. S5 Schematic diagram of two transmitter and three receiver model.

Here, $\gamma_n(n = 1,2,3)$ represents the rate of the receiver feeding system, $\Gamma_n(n = 1,2,3)$ is the intrinsic loss of each receiver, and $\kappa_n(n = 1,2,3)$ is the coupling rate between the transmitter and each receiver. To simplify the model, we set $\gamma_1 = \gamma_2 = \gamma_3 = \gamma$, $\Gamma_1 = \Gamma_2 = \Gamma_3 = \Gamma$, $\kappa_1 = \kappa_2 = \kappa_3 = \kappa$, and $g_1 = g_2 = g$. Under zero reflection conditions $S_{1-} = -S_{1+} + \sqrt{2g_1}a_1 + \sqrt{2g_2}a_2 = 0$, we can obtain its Hamiltonian as follows:

$$H_5 = \begin{pmatrix} \omega_0+\delta+ig-\Gamma & \kappa & \kappa & \kappa & ig \\ \kappa & \omega_0-i\gamma-\Gamma & 0 & 0 & -\kappa \\ \kappa & 0 & \omega_0-i\gamma-\Gamma & 0 & -\kappa \\ \kappa & 0 & 0 & \omega_0-i\gamma-\Gamma & -\kappa \\ ig & -\kappa & -\kappa & -\kappa & \omega_0-\delta+ig-\Gamma \end{pmatrix} \tag{S5}$$

At this point, when the system is operated, it satisfies the condition: $(PT)\boldsymbol{H}_5(PT)^{-1} = -\boldsymbol{H}_5$, meaning that this fifth-order system also satisfies anti-PT- symmetry.